

Calculations with the nuclear firestreak model*

J. Gosset,[†] J. I. Kapusta, and G. D. Westfall

Lawrence Berkeley Laboratory, Berkeley, California 94720

(Received 27 March 1978)

A model is presented which is capable of calculating simultaneously the spectra of pions, nucleons, and light nuclei from the collision of relativistic heavy ions. It is based on the nuclear thermodynamics of Mekjian and Kapusta. Maximum use is made of the conservation laws for baryon number, charge, energy, momentum, and angular momentum. Single particle inclusive cross sections were calculated and compared with experiment for a wide range of beam energies and observed fragments. Except for some conflicting normalizations and high-energy pions good agreement is found. The density at which hadrons effectively cease to interact, which is the only parameter in the model, is determined to be 0.12 hadrons/fm³.

NUCLEAR REACTIONS Relativistic heavy ions; firestreaks, hadronic thermal equilibrium; calculated differential cross sections of π^+ , p , d , t , ^3He , ^4He ; comparisons with experiment.

I. INTRODUCTION

Recently a large amount of experimental data concerning relativistic heavy ion reactions has become available.¹⁻⁴ The data considered here consist of single particle inclusive spectra of pions, nucleons, and light nuclei up to ^4He . These spectra were measured for a variety of target-projectile-incident energy combinations over a wide range of observed energies and angles. Several models⁵ have been proposed to predict the nucleon spectra produced in these collisions including the nuclear fireball model,⁶ the firestreak model,⁷ intranuclear cascade,⁸⁻¹⁰ hydrodynamics,⁹⁻¹¹ row on row,¹² and nucleon knockout.¹³ The light nuclei spectra have been interpreted in terms of the coalescence model,¹⁴ equilibrium thermodynamics,¹⁵ and the sudden approximation in quantum mechanics.¹⁶ An explanation of the low-energy pion spectra has been attempted in terms of the superposition of proton-nucleus results. Pion production has also been interpreted within the framework of the fireball model.¹⁷

It is hoped that in relativistic heavy ion collisions, new phenomena can be studied such as density isomers or pion condensates.¹⁸ However, the calculation of observable quantities resulting from these exotic phenomena are not yet possible. A calculation incorporating known phenomena would be useful in predicting what one would expect to observe in these reactions if nothing unusual were taking place. Such a model must be simple enough to allow comparison with data and yet must include enough realistic features to make a comparison reasonable. These features should include a description of the size and shape of nuclei, incorporation of conservation laws, and the concept

that many "interactions" take place during the collision.

Presented here is a macroscopic model capable of simultaneously predicting the pion, nucleon, and light nucleus inclusive spectra resulting from relativistic heavy ion collisions. The model is based on the geometrical and kinematical assumptions used in the firestreak model⁷ including diffuse nuclear density distributions. Also included is equilibrium thermodynamics^{15,17} solved self-consistently to obtain the relative concentrations and distribution functions of the various particles produced in these collisions. This model will be referred to as "the nuclear firestreak model."

In Sec. II a detailed description of the model is presented followed by a comparison to the existing data in Sec. III.

II. DESCRIPTION OF THE MODEL

The basic philosophy is similar to the one in the nuclear fireball model⁶ which was used to calculate the proton inclusive spectra from relativistic heavy ion collisions. One assumed that there were enough "interactions" for thermodynamic equilibrium to occur between the nucleons that participate in the reaction. These nucleons form a fireball which decays as an ideal gas. This simple model is deficient in two significant respects. First, it is necessary to explain not only the production of nucleons in these collisions but also the copious production of the composite fragments as well as of pions. The thermodynamic equilibrium between nucleons has been generalized to a chemical equilibrium between the various hadronic species through the use of a chemical potential.^{15,17} The one variable parameter which has been in-

troduced in the model is the critical density at which equilibrium is reached and below which the momentum distribution of the fragments does not vary because they are no longer interacting. This critical density has also been called the freeze-out or breakup¹⁶ density. The second deficiency is the drastic geometrical assumptions used in the nuclear fireball model of sharp spheres and clean cylindrical cuts between the colliding nuclei. The treatment of nuclear density distributions with diffuse surfaces⁷ leads to a temperature gradient across the fireball according to the relative amounts of material coming from the target and the projectile.

Thus the model describes relativistic heavy ion collisions by assuming that the interaction between the nuclei is localized to the overlapping volume. In this volume the interaction proceeds via colinear streaks of nuclear matter from the target and projectile that undergo completely inelastic collisions. This nuclear matter is treated as a thermodynamic system in chemical equilibrium which allows the calculation of the relative concentrations of pions, nucleons, and light nuclei and their distribution functions. The firestreak geometry explicitly conserves angular momentum whereas it is well known that the fireball geometry does not. At low energy ($\lesssim 1$ GeV/nucleon) this angular momentum nonconservation is not an important effect, whereas at high energy it is. Of course, in this model one cannot investigate the detailed time development of the collision since there are no equations of motion.

In this section we present the model in detail with respect to the geometry and kinematics first, and then to the thermodynamics.

A. Geometry and kinematics

To treat nuclear density distributions with diffuse surfaces one can subdivide the projectile and target into infinitesimal streaks parallel to the relative motion of the colliding nuclei.⁷ Each of these streaks is characterized completely by the relative amount η of material coming from the projectile. Here $\eta = N_p / (N_p + N_t)$ where N_p and N_t are the number of contributing nucleons from the projectile and target. It should be noted that η is, in principle, a continuous variable, but for computational purposes is taken to be discrete. The velocity β of the streak center of mass and its rest mass M depend only on this parameter η . The expression for calculating any observable involves in principle a double summation over this parameter η and over the impact parameter. Since η defines completely the collision for any single particle observable, this double summation

can be partially done over the impact parameter.¹⁹ The Lorentz invariant momentum space densities F_j for particles of type j which are produced in the collision can be expressed as a sum of terms, each of which is factorized into a geometrical part, which is the yield function $Y(\eta)$, and the Lorentz invariant momentum space density f_j for particles of type j emitted by a system of mass $M(\eta)$ moving in the laboratory at the velocity $\beta(\eta)$:

$$F_j(\vec{p}) = \sum_{i=1}^N Y(\eta_i) f_j[\vec{p}; M(\eta_i), \beta(\eta_i)]. \quad (1)$$

The yield function Y , in units of cross section, contains all the geometrical aspects of the problem.

One defines $w_b(x, y)$ as the combined target-projectile density distribution projected onto the x - y plane perpendicular to the beam. The yield function is calculated by integrating $w_b(x, y)$ over impact parameter b and over the x - y plane:

$$Y(\eta_i) = \int_{\eta_i - 1/2\delta\eta}^{\eta_i + 1/2\delta\eta} d\eta' \int 2\pi b db \iint dx dy w_b(x, y) \times \delta[\eta' - \eta_b(x, y)]. \quad (2)$$

Throughout this paper the yield functions tabulated in Ref. 7 will be used.

Each term of the summation (1) corresponds to a streak having a charge to baryon number ratio Q/B of

$$\frac{Q}{B} = \eta \frac{Z_p}{A_p} + (1 - \eta) \frac{Z_t}{A_t}, \quad (3)$$

where Z_i and A_i are, respectively, the charge and baryon numbers of the projectile ($i=p$) and target ($i=t$) nuclei. The laboratory velocity of the streak center of mass is

$$\beta = \frac{P_{\text{lab}}}{E_{\text{lab}}}. \quad (4)$$

P_{lab} and E_{lab} are the laboratory momentum and total energy of the streak. This velocity can be rewritten in terms of η as

$$\beta = \frac{\eta [t(t + 2m')]^{1/2}}{m' + \eta t}. \quad (5)$$

Here t is the laboratory kinetic energy per nucleon of the projectile and m' is the bound nucleon mass. The rest mass of the streak is

$$M = (E_{\text{lab}}^2 - P_{\text{lab}}^2)^{1/2}, \quad (6)$$

which can also be rewritten in terms of η as

$$\frac{M}{B} = m' \left(1 + 2\eta(1 - \eta) \frac{t}{m'} \right)^{1/2}. \quad (7)$$

Taking into account the neutron-proton mass difference, which has been done in the calculations

presented in this paper, leads to slightly more complicated formulas than Eqs. (5) and (7) for β and M .

B. Thermodynamics

The Lorentz invariant momentum space densities f_j can be calculated in any reference frame, in particular in the streak center of mass frame where \vec{p} is Lorentz transformed into \vec{p}' and β is

equal to zero:

$$f_j[\vec{p}; M(\eta_i), \beta(\eta_i)] = f_j[\vec{p}'; M(\eta_i), 0]. \quad (8)$$

These momentum space densities follow from the assumption of thermodynamic equilibrium between all possible nuclear species at the given critical hadron density ρ_c . They are isotropic in the streak center of mass frame with a Fermi or Bose distribution:

TABLE I. Grouping of nuclear resonances into effective resonances used in the calculations.

Nucleus	Excitation energy above g.s.	J^P	Decay modes	Effective decay mode	$\frac{\sum_i (2S_i + 1) E_i}{\sum_i (2S_i + 1)}$	$\sum_i (2S_i + 1)$
					effective Ex. energy	effective (2S+1)
${}^2\text{H}$	2.2	1^+	$p+n$	$p+n$	2.2	Boson 3
${}^4\text{H}$	0(-5.1) ^a	2^-	${}^3\text{H}+n$			Boson
	1.7	1^-	${}^3\text{H}+n$	${}^3\text{H}+n$	1.6	11
	4.1	1^-	${}^3\text{H}+n$			
${}^4\text{He}$	20.1	0^+	p			
	21.1	0^-	p, n	$\frac{1}{2}({}^3\text{He}+n)$		Boson
	22.1	2^-	p, n	+		
	25.5	0^+	\dots	$\frac{1}{2}({}^3\text{H}+p)$	27.5	
	26.4	2^-	p, n			28
	27.4	1^-	p, n, γ			
	29.5	0^-	p, n			
	30.5	1^-	p, n, γ			
	31.0	1^-	p, n, d			
	33.0	2^+	p, n, d			
${}^4\text{Li}$	0(-3.0) ^a	2^-	${}^3\text{He}+p$			Boson
	1.4	1^-	${}^3\text{He}+p$	${}^3\text{He}+p$	1.9	12
	3.2	0^-	${}^3\text{He}+p$			
	5.0	1^-	${}^3\text{He}+p$			
${}^5\text{He}$	0(0.9) ^a	$\frac{3}{2}^-$	n, α			Fermion
	4.0	$\frac{1}{2}^-$	n, α	${}^4\text{He}+n$	11.1	14
	16.8	$\frac{3}{2}^+$	γ, n, d, t, α			
	19.9	$\frac{3}{2}^+$	n, d, t, α			
${}^5\text{Li}$	0(1.9) ^a	$\frac{3}{2}^-$	p, α			Fermion
	4.0	$\frac{1}{2}^-$	p, α	${}^4\text{He}+p$	11.9	16
	16.7	$\frac{3}{2}^+$	$\gamma, p, d, {}^3\text{He}, \alpha$			
	18.0	$\frac{1}{2}^+$	$\gamma, p, d, {}^3\text{He}, \alpha$			
	20.0	$\frac{3}{2}^+$	$\gamma, p, d, {}^3\text{He}, \alpha$			

^a The numbers in parentheses refer to the binding energy with respect to the constituent nucleons.

$$f_j(\vec{p}') = E' \frac{d^3 N_j}{d^3 p'^3} = E' \frac{(2S_j + 1)V}{(2\pi)^3} \left(\exp \frac{E' - \mu_j}{T} \pm 1 \right)^{-1} \quad (9a)$$

$$- E' \frac{(2S_j + 1)V}{(2\pi)^3} \exp \left(\frac{\mu_j - m_j}{T} \right) \exp \left(\frac{-p'^2}{2m_j T} \right). \quad (9b)$$

The arrow indicates the classical statistics non-relativistic limit. The quantity m_j is the mass of the particle, E' its total energy equal to $(p'^2 + m_j^2)^{1/2}$, and S_j and μ_j its spin and chemical potential. V and T are, respectively, the volume and the temperature of the system at the critical density. The + or - sign refers to fermion or bosons. We use $\hbar = c = k = 1$.

The statement of thermal equilibrium implies certain relations among the chemical potentials. For example $n + n + p \rightleftharpoons n + d$ implies that $\mu_d = \mu_n + \mu_p$ and $p + n \rightleftharpoons n + n + \pi^+$ implies that $\mu_{\pi^+} = \mu_p - \mu_n$. The chemical potentials of all the hadrons are linear combinations of the neutron and proton chemical potentials μ_n and μ_p . Since we want to calculate composite particle production up to ${}^4\text{He}$, as well as pion production, it is necessary to include in the chemical equilibrium at least pions, neutrons, protons, deuterons, tritons, ${}^3\text{He}$, and ${}^4\text{He}$. It is well known that at the energies considered in this paper, pion production proceeds mainly

through the formation and decay of the Δ resonance. This baryonic resonance is taken into account in the chemical equilibrium with its four charge states. In contrast to Ref. 17 the wide mass spectrum of the Δ is approximated by nine discrete masses at regular intervals from threshold and symmetrically arranged around the central value of 1232 MeV. Each mass is given a weight from a single-level resonance formula²⁰ and the total weight is normalized to 1. Since a species with such a short lifetime is introduced in the system we should also take into account the effect of the excited unbound states of composite fragments, as already suggested in Ref. 15, up to mass 5 for calculating ${}^4\text{He}$ production. Because of their great number²¹⁻²³ they are grouped together as shown in Table I with an effective excitation energy, degeneracy $(2S + 1)$, and decay mode(s) for each one of the nuclear species ${}^2\text{H}$, ${}^4\text{H}$, ${}^4\text{He}$, ${}^4\text{Li}$, ${}^5\text{He}$ and ${}^5\text{Li}$. These resonances, baryonic as well as nuclear, are supposed to leave the equilibrium region intact and naturally decay afterwards by particle emission into pions, nucleons, and stable-light nuclei. The stable particle spectra thus consist of a sum of two components, a thermal one given by Eq. (9) and a resonance two-body decay one, resulting from all the possible two-body decays of resonances which are themselves emitted with a thermal spectrum given by Eq. (9). As shown in Ref. 17, this second component can be written

$$f_j(\vec{p}') = \sum_R \frac{W_D(2S_R + 1)V m_R T^2}{16\pi^3 p' p_D} \left(\frac{\mu_R}{T} \ln(1 + e^{-x}) + \sum_{n=1}^{\infty} \frac{(\mp)^{n+1}}{n^2} e^{-nx} (nx + 1) \right) \Big|_{x_+}^{x_-}, \quad (10)$$

where

$$Tx_{\pm} = \frac{m_R}{m_j} (E' E_D \pm p' p_D) - \mu_R. \quad (11)$$

Here S_R , m_R , and μ_R are the spin, mass, and chemical potential of the resonance R . W_D is the branching ratio for the decay of the resonance R into the particle of type j . The quantities p_D and E_D are the decay momentum and total energy of the particle of type j in the rest frame of the resonance R .

The thermodynamical problem can thus be summarized in the following way. For each value of the projectile relative amount η we have to find the neutron and proton chemical potentials μ_n and μ_p , the temperature T and the volume V of a system in thermodynamical equilibrium with baryon number B , charge Q , and total mass M at hadron density ρ_c . The total number N_j and average E_j (including rest mass) of each type j of particle or

resonance can be obtained by integrating Eq. (9) with the proper integrand:

$$N_j = \frac{(2S_j + 1)V m_j^2 T}{2\pi^2} \sum_{n=1}^{\infty} \frac{(\mp)^{n+1}}{n} \exp \frac{n\mu_j}{T} K_2 \left(\frac{n\mu_j}{T} \right) \quad (12a)$$

$$- (2S_j + 1)V \left(\frac{m_j T}{2\pi} \right)^{3/2} \exp \left(\frac{\mu_j - m_j}{T} \right) \quad (12b)$$

and

$$N_j E_j = \frac{(2S_j + 1)V m_j^3 T}{2\pi^2} \times \sum_{n=1}^{\infty} \frac{(\mp)^{n+1}}{n} \exp \left(\frac{n\mu_j}{T} \right) \left[K_1 \left(\frac{n\mu_j}{T} \right) + \frac{3T}{n\mu_j} K_2 \left(\frac{n\mu_j}{T} \right) \right] \quad (13a)$$

$$- N_j (m_j + \frac{3}{2}T). \quad (13b)$$

The volume dependence is very simple. The number and energy densities depend only on the three

variables μ_n , μ_p , and T . For any set of values of these variables, it is possible to calculate the baryon (b), charge (q), energy (e), and hadron (h) densities:

$$b(\mu_n, \mu_p, T) = \sum_j \left(\frac{N_j}{V} \right) B_j, \quad (14)$$

$$q(\mu_n, \mu_p, T) = \sum_j \left(\frac{N_j}{V} \right) Q_j, \quad (15)$$

$$e(\mu_n, \mu_p, T) = \sum_j \left(\frac{N_j}{V} \right) E_j, \quad (16)$$

and

$$h(\mu_n, \mu_p, T) = \sum_j \frac{N_j}{V} H_j, \quad (17)$$

where B_j , Q_j , and H_j are the baryon, charge, and hadron quantum numbers of particles or resonances of type j . There remain only three equations to be solved for μ_n , μ_p , and T , for example:

$$\begin{aligned} e/b &= M/B, \\ q/b &= Q/B, \\ h &= \rho_c \end{aligned} \quad (18)$$

and the volume V will follow from the solution to these equations, being simply equal to B/b . The system of Eqs. (18) is not linear in μ_n , μ_p , and T . It is solved by a least squares method, minimizing the function:

$$\chi^2(\mu_n, \mu_p, T) = \left(\frac{e/b}{M/B} - 1 \right)^2 + \left(\frac{q/b}{Q/B} - 1 \right)^2 + \left(\frac{h}{\rho_c} - 1 \right)^2, \quad (19)$$

with the starting guess being the classical statistics, nonrelativistic case with only nucleons.²⁴

III. COMPARISON WITH EXPERIMENT

In this section, the predictions of the nuclear firestreak model will be compared with most of the available data on single particle inclusive differential cross sections. These comparisons cover beam energies from 400 to 2100 MeV per nucleon (MeV/nucleon). The observed fragments range from π to ${}^4\text{He}$ depending on the experiment. All of the calculations presented here were performed with the same value of the critical density ρ_c which will be discussed below. All of the calculations were performed including both the ground and excited states of the light nuclei and including pions as discussed in Sec. II. The effect of neglecting the excited states will be discussed below. Finally, the range of the variable η appearing in the yield function $Y(\eta)$ was taken to be beam energy dependent. The value of η_{\min} (with $\eta_{\max} = 1 - \eta_{\min}$)

was chosen so that the resultant excitation energy per baryon was 5 to 10 MeV into the continuum. The part of $Y(\eta)$ which is not included contributes predominantly to the yield of higher mass nuclear fragments and thus is outside the scope of this paper. Although one may question the wisdom of discussing such fine points in a model as simple as this one, nonetheless, it is fruitful to examine the consequences of a consistent application of any model to pinpoint precisely those regions where the model fails.

First consider the bombardment of ${}^{238}\text{U}$ by a 400 MeV/nucleon ${}^{20}\text{Ne}$ beam.¹ The double differential cross section at fixed laboratory angle as a function of laboratory kinetic energy per nucleon for p , d , t , ${}^3\text{He}$, and ${}^4\text{He}$ is shown in Figs. 1 through 5, respectively. All of the theoretical curves have been multiplied by a factor of 2, except for the special case of ${}^4\text{He}$ which will be discussed separately below.

The agreement of the calculated curves with the shape of data is excellent in all cases except for the 30° spectra. The shapes of the cross sections are essentially independent of the value of ρ_c . The magnitudes of the cross sections are somewhat dependent on ρ_c , the heavier the nuclear fragment

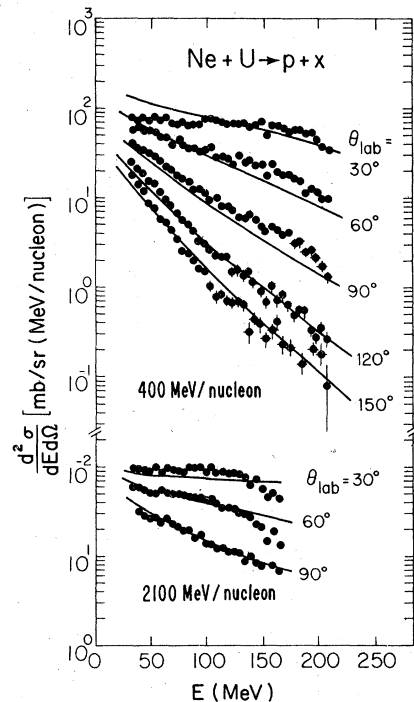


FIG. 1. Spectra of protons in the lab from the bombardment of U by Ne at 400 and 2100 MeV/nucleon. Data are from Ref. 1. See text concerning the 2100 MeV/nucleon data. The model predictions have been multiplied by 2.

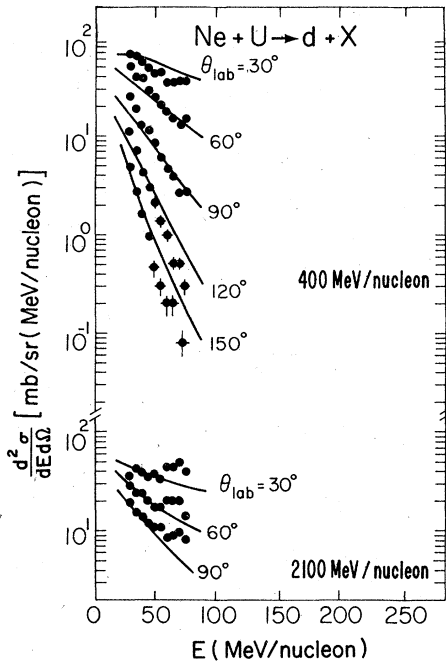


FIG. 2. Spectra of deuterons in the lab from the bombardment of U by Ne at 400 and 2100 MeV/nucleon. Data are from Ref. 1. See text concerning the 2100 MeV/nucleon data. The model predictions have been multiplied by 2.

the stronger the dependence. As ρ_c is increased over a reasonable range of values, the d yield decreases while the ${}^4\text{He}$ yield increases. A unique value of $\rho_c = 0.12 \pm 0.02$ hadrons/ fm^3 was found for which the normalization discrepancy between theory and experiment was the same for p , d , t , and ${}^3\text{He}$. Certainly there is no *a priori* reason to believe that such a value should exist. Indeed our attempt to fit the data by including only the bound light nuclei does not result in a unique value of ρ_c . It is significant that this density is slightly less than normal nuclear density because this allows the interpretation that some of the nucleons condense into composite states in a statistical manner when the density is low enough. These observations lend credence to the whole concept of light nuclei, both ground state and excited, being in thermal equilibrium at some critical density. In fact the fit is so good, considering that there is only one adjustable parameter,²⁵ that one should seriously entertain the possibility that the absolute normalization of the experiment is too high by a factor of 2. The estimated uncertainty in the absolute normalization was 30%. This would be a 1.7 standard deviation departure. If subsequent measurements confirm this normalization discrepancy then one must conclude that the model is missing some essential physics.

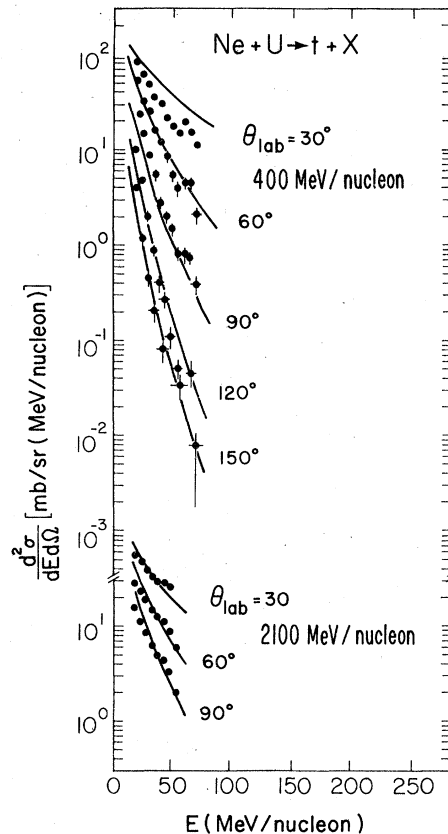


FIG. 3. Spectra of tritons in the lab from the bombardment of U by Ne at 400 and 2100 MeV/nucleon. Data are from Ref. 1. See text concerning the 2100 MeV/nucleon data. The model predictions have been multiplied by 2.

The theoretical curve for ${}^4\text{He}$ shown in Fig. 5 was multiplied by a factor of 4. This additional factor of 2 may arise from several effects. First, a cutoff has been placed at $A=5$. The $A=4$ nucleus is most sensitive to this cutoff with the $A=1, 2, 3$ nuclei being less sensitive. In addition, ${}^4\text{He}$ is an exceptionally stable nucleus. Therefore many unstable higher mass states decay into ${}^4\text{He}$ but less so into d , t , or ${}^3\text{He}$. Thus, depending on what aspects of the reaction one wishes to study, ${}^4\text{He}$ is or is not a good tool for investigation.

It should be noted in passing that the same calculations performed with the fireball geometry instead of the firestreak geometry with diffuse nuclear surfaces cannot reproduce the data on d , t , ${}^3\text{He}$, and ${}^4\text{He}$ even in overall shape. This is true for all the data examined in this paper. This illustrates the importance of the diffuse nuclear surface in the model.

²³⁸U was also bombarded by ²⁰Ne at 2100 MeV/nucleon.¹ There were experimental diffi-

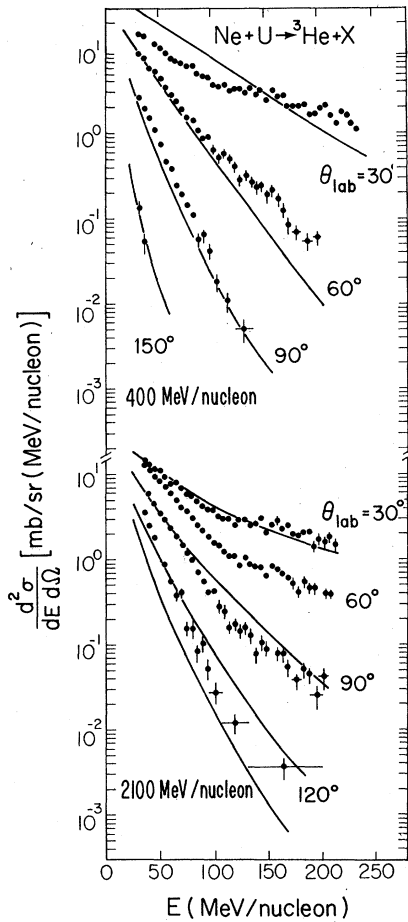


FIG. 4. Spectra of ${}^3\text{He}$ in the lab from the bombardment of U by Ne at 400 and 2100 MeV/nucleon. The model predictions have been multiplied by 2. Data are from Ref. 1.

culties with the detection of p , d , and t but not of ${}^3\text{He}$ and ${}^4\text{He}$. The shape of the cross section at a given angle was measured reliably but the normalization changed from run to run by factors of 2 or so. The 2100 MeV/nucleon data on p , d , and t shown in Figs. 1 to 3 was renormalized angle by angle from the original presentation of portions of it.²⁶ To be consistent with the 400 MeV/nucleon comparison the theoretical curves have been uniformly multiplied by a factor of 2, except for ${}^4\text{He}$ which has been multiplied by a factor of 6. Thus we do not claim detailed agreement between theory and experiment. All we claim is that the shapes of the cross sections at given angle agree and that normalizations are well within an order of magnitude.

However, the angular distribution predicted by the model for ${}^3\text{He}$ and ${}^4\text{He}$ disagrees with the observed angular distribution which should be ex-

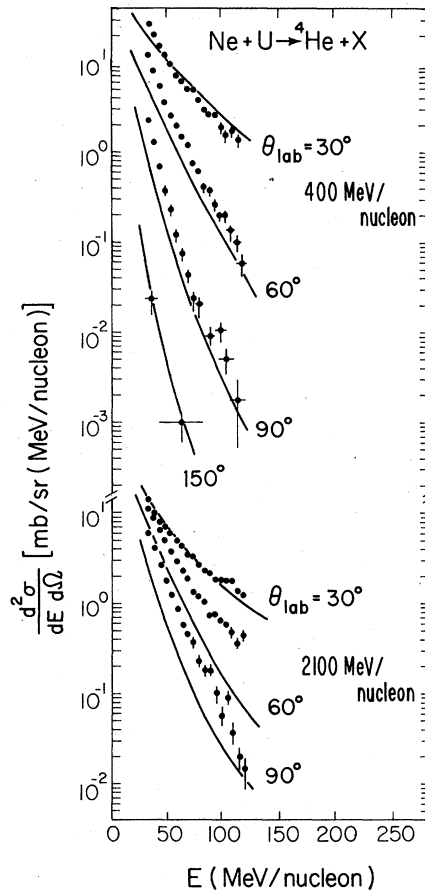


FIG. 5. Spectra of ${}^4\text{He}$ in the lab from the bombardment of U by Ne at 400 and 2100 MeV/nucleon. Data are from Ref. 1. The model predictions have been multiplied by a factor of 4 and 6, respectively.

perimentally reliable. The theory seems to reproduce the difference between the 30° and 120° spectra but underestimates the 60° and 90° spectra.

The fragments p , d , and t from the bombardment of ${}^9\text{Be}$ and ${}^{63}\text{Cu}$ by an 1800 MeV/nucleon ${}^{40}\text{Ar}$ beam were measured in a recent experiment.² The Lorentz invariant cross section at given laboratory angle as a function of laboratory momentum is shown in Figs. 6 to 8. The data and theory are shown with their absolute normalizations unchanged. The experimental absolute normalization uncertainties are estimated as 25% for Be and 10% for Cu. The critical density is $\rho_c = 0.12$ hadrons/fm³ although the results do not change much if ρ_c is varied from 0.10 to 0.14. The model seems to represent the data fairly well at 14.7° although the tritons from Cu may be a little underestimated. At 5° , however, the model generally

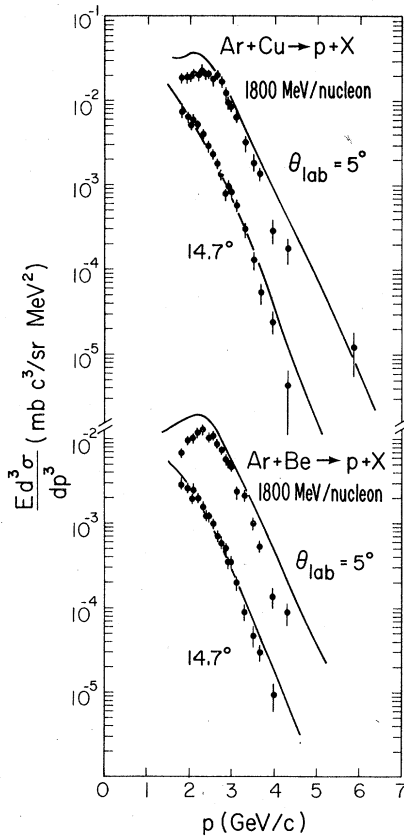


FIG. 6. Invariant cross section vs lab momentum for protons from the bombardment of Cu and Be by Ar at 1800 MeV/nucleon. Data are from Ref. 2.

overestimates the data especially in the more central region corresponding roughly to 2 GeV/c for protons, 3 GeV/c for deuterons, and 4 GeV/c for tritons. This could be caused by a variety of mechanisms but the most obvious one should be mentioned. It could be that the assumption of completely inelastic collisions between tubes is breaking down and that the surfaces of the colliding nuclei are somewhat transparent. This would tend to decrease the cross sections at the most forward angles where the main contribution comes from less central collisions.

Finally, we compare with the high-energy protons and pions³ and the low-energy pions⁴ from the bombardment of NaF and ²⁰⁸Pb by ²⁰Ne at a beam energy of 800 MeV/nucleon. The uncertainty in absolute normalization is estimated at around 25% for both sets of data. The higher energy data are plotted in Figs. 9 to 12 in the form of the Lorentz invariant differential cross section as a function of rapidity at fixed transverse momentum. This is a Lorentz invariant way of presenting

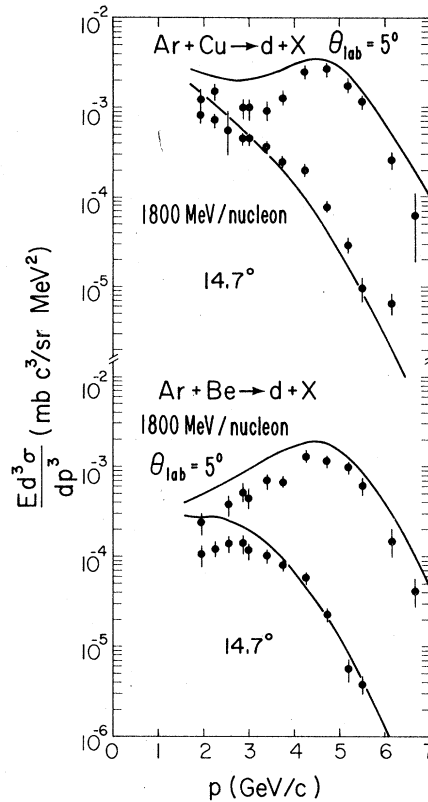


FIG. 7. Invariant cross section vs lab momentum for deuterons from the bombardment of Cu and Be by Ar at 1800 MeV/nucleon. Data are from Ref. 2.

data over a large kinematic region. A Lorentz transformation along the beam axis just shifts all rapidities by a constant amount. Figures 13 and 14 show the low-energy pions in the more conventional plot of double differential cross section as a function of energy at fixed laboratory angle. Figures 9 to 12 show the absolute normalization of both theory and experiment, whereas the theoretical curves in Figs. 13 and 14 have been multiplied by $\frac{1}{2}$. The model gives a good representation of the protons from Pb, but generally overestimates them from the much smaller target NaF although the shapes agree quite well.

The model overestimates the cross section for pion production as is evident from both the low- and high-energy data. Looking at the low energy pions note that the model does not give enough curvature in the spectrum. A larger curvature is indicative of forward-backward peaking which is more characteristic of elementary nucleon-nucleon collisions. Further analysis⁴ shows that the shape of the spectrum is not consistent with the free space reaction $NN \rightarrow NN\pi$ either. Thus the pions are probably rescattering to some extent

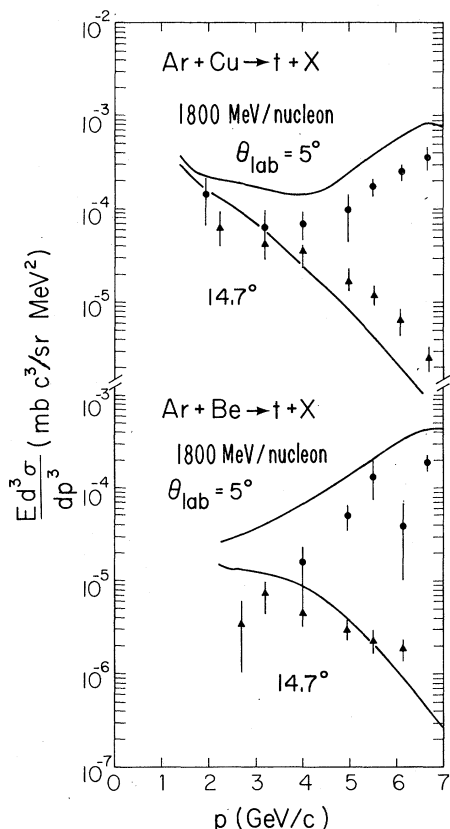


FIG. 8. Invariant cross section vs lab momentum for tritons from the bombardment of Cu and Be by Ar at 1800 MeV/nucleon. Data are from Ref. 2.

but not enough to reach thermal equilibrium. Consideration of the high-energy pions leads to the same conclusion. More experiments need to be done with larger mass projectiles on Pb or U at various beam energies to get as far away as possible from the elementary $NN \rightarrow NN\pi$ reaction.

Finally, we can examine three quantities which in some sense summarize the calculations. Figure 15 shows the temperature as a function of η for the beam energies 400, 800, and 2100 MeV/nucleon. (The 1800 MeV/nucleon calculation is not shown.) Near the target ($\eta \approx 0$) and projectile ($\eta \approx 1$) the temperature is lowest because the available center of mass energy is less in those regions. Inclusion of pions and Δ 's lowers the temperature, especially at the higher beam energies since energy is required to create these particles. Inclusion of the light nuclei raises the temperature somewhat. This is because the binding of nucleons into nuclei converts mass energy to random motion, and the number of degrees of freedom in the system becomes smaller so that the

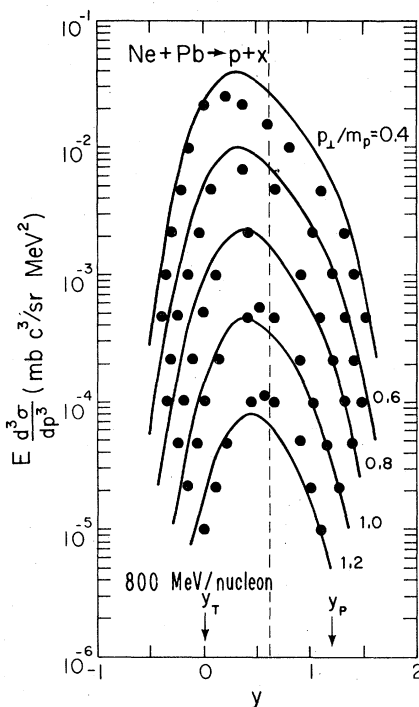


FIG. 9. Invariant cross section vs rapidity at fixed transverse momentum for protons from the bombardment of Pb by Ne at 800 MeV/nucleon. The dashed line represents the nucleon-nucleon center of mass frame. Error bars (not shown) range from 20% for the large cross sections to 100% for the small cross sections. Data are from Ref. 3.

energy per degree of freedom is higher. Note that the temperatures shown do not correspond precisely to effective temperatures measured in the laboratory because when the particles go out of thermal equilibrium the resonances decay and so add some net kinetic energy to the final state. Figure 16 shows the ratio of the number of nucleons to the baryon number in the final state, i.e., after all resonances have decayed. This ratio is smallest near the target and projectile where the temperatures are low. The formation of light nuclei is favored when the temperature is low. This graph nicely illustrates how much error is involved in neglecting the production of light nuclei. At 400 MeV/nucleon at least 35% of the baryon number is bound up in light nuclear fragments! Figure 17 shows the ratio of the number of pions to the baryon number in the final state. This ratio increases with beam energy. Also it is peaked in the central region where the available center of mass energy, and hence the temperature, is the highest.

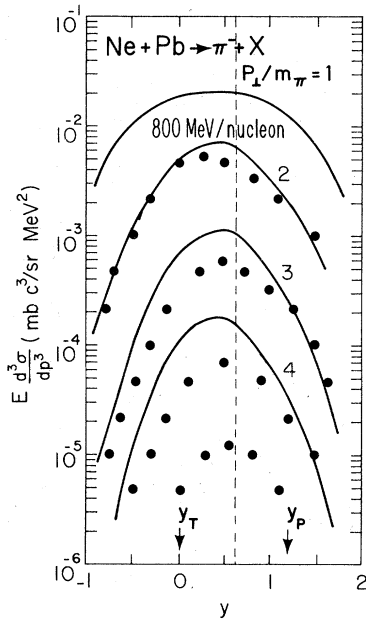


FIG. 10. Invariant cross section vs rapidity at fixed transverse momentum for negative pions from the bombardment of Pb by Ne at 800 MeV/nucleon. The dashed line represents the nucleon-nucleon center of mass frame. Error bars (not shown) range from 20% for the large cross sections to 100% for the small cross sections. Data are from Ref. 3.

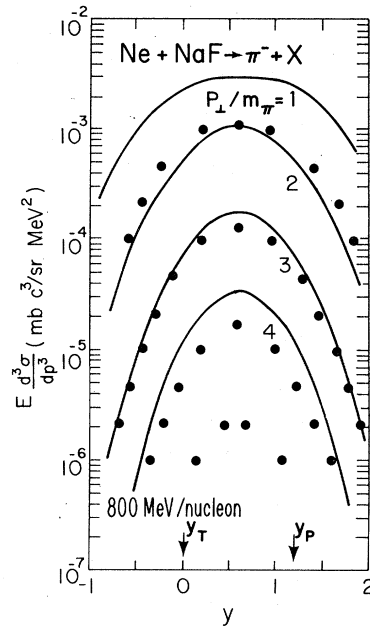


FIG. 12. Invariant cross section vs rapidity at fixed transverse momentum for negative pions from the bombardment of NaF by Ne at 800 MeV/nucleon. Error bars (not shown) range from 20% for the large cross sections to 100% for the small cross sections. Data are from Ref. 3.

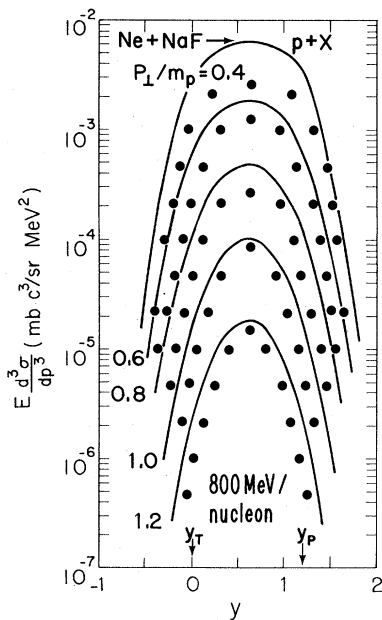


FIG. 11. Invariant cross section vs rapidity at fixed transverse momentum for protons from the bombardment of NaF by Ne at 800 MeV/nucleon. Error bars (not shown) range from 20% for the large cross sections to 100% for the small cross sections. Data are from Ref. 3.

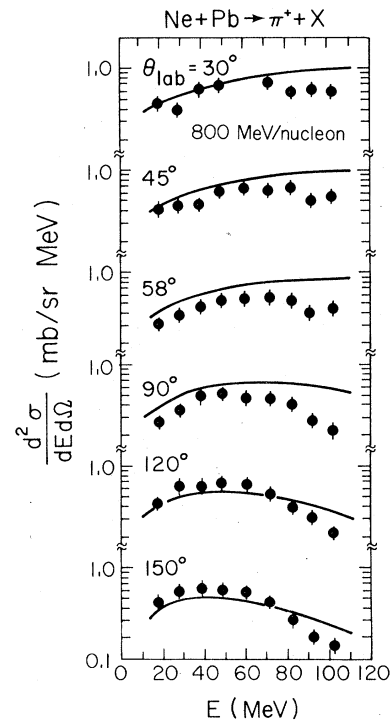


FIG. 13. Spectra of positive pions in the lab from the bombardment of Pb by Ne at 800 MeV/nucleon. Data are from Ref. 4. The model predictions have been multiplied by $\frac{1}{2}$.

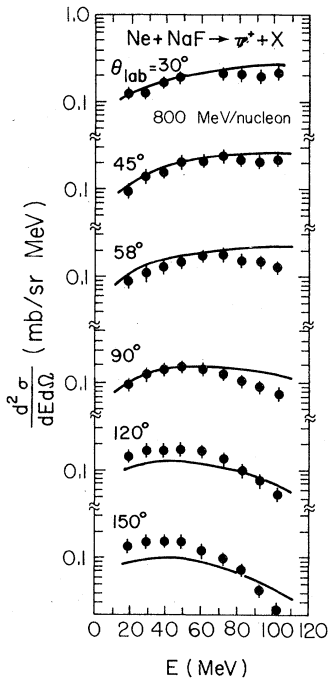


FIG. 14. Spectra of positive pions in the lab from the bombardment of NaF by Ne at 800 MeV/nucleon. Data are from Ref. 4. The model predictions have been multiplied by $\frac{1}{2}$.

IV. CONCLUSION

The nuclear firestreak model predicts, with a large degree of success, the pion, nucleon, and light nucleus inclusive spectra from a large variety of projectile-target-incident energy combinations over a wide kinematic range. The simultaneous prediction of the pion, nucleon, and light nucleus spectra is in contrast to models such as hydrodynamics where only the nucleon spectra can be predicted, intranuclear cascade which can

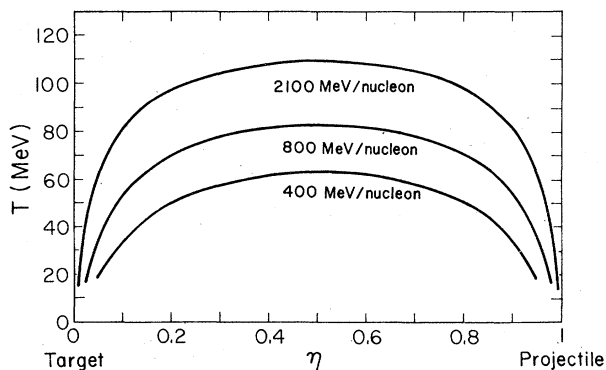


FIG. 15. Temperature vs η for three bombarding energies.

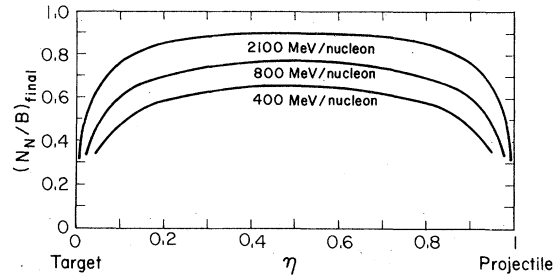


FIG. 16. Ratio of the number of nucleons to the baryon number in the final state vs η .

only predict pions and nucleons, or the coalescence model which predicts the light nuclei spectra based on the measured proton spectra.

The model incorporates one variable parameter, the freeze-out density, ρ_c , which is uniquely determined to be 0.12 ± 0.02 hadrons/fm³. The model, however, says nothing about densities greater than ρ_c except that it assumes that the expansion from the initial compressed state to the breakup density is isoergic.

The diffuse nuclear density distributions incorporated in this model are necessary to reproduce the shape of the measured spectra, especially for the light nuclei. However, the pion spectra is insensitive to whether or not one uses diffuse nuclear surfaces. Light nuclei are produced primarily in those regions which have a dominant amount of matter coming from either the target ($\eta \approx 0$) or projectile ($\eta \approx 1$), whereas the pions are primarily produced in those regions in which the target and projectile contribute equal amounts ($\eta \approx \frac{1}{2}$).

Consideration has been given to the breakdown of some of the assumptions in the model. The assumption of straight line trajectories could break down, producing conical rather than cylindrical cuts through the nuclei. This effect would involve transverse spreading of the interaction region. The assumption of full momentum transfer between the tubes must break down in large

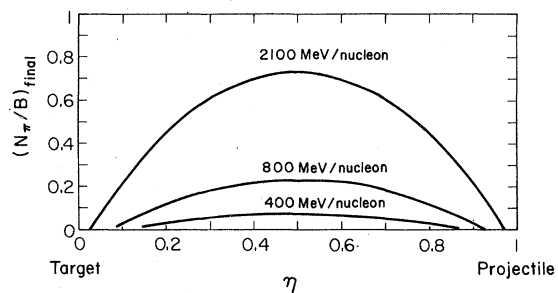


FIG. 17. Ratio of the number of pions to the baryon number in the final state vs η .

impact parameter collisions where the two nuclei interact only through the diffuse tails of their density distributions. The inclusion of transparency or the treatment of these types of tubes in terms of nucleon-nucleon scattering could be incorporated. The model also does not consider pre-equilibrium emission. This effect would most strongly affect the pion spectra.

One can predict multiparticle correlations using this model as well as multiplicity distributions.²⁷ However, to obtain these results, it seems to be necessary to return to the full two dimensional integral over impact parameter and η .

The exact quantum field theory treatment of relativistic heavy ion reactions is probably not a realistic goal. However, the relatively good suc-

cess of the nuclear firestreak model may help point the way toward more comprehensive models or theories of these reactions.

ACKNOWLEDGMENTS

We are grateful to numerous members of the Nuclear Science Division of LBL for their critical comments and thought provoking questions regarding this work. In particular we thank W. D. Myers for allowing us the use of his computer code. We thank the authors of the experimental work (Refs. 1-4) for their cooperation and for allowing us to publish their results. For their carefully considered reading of the manuscript we thank W. D. Myers and A. M. Poskanzer.

*This work was supported by Nuclear Physics Division of the U. S. Department of Energy.

†Permanent address: DPhN/Me, Centre d'Etudes Nucleaires de Saclay, 91190 Gif-sur-Yvette, France.

¹J. Gosset, H. H. Gutbrod, W. G. Meyer, A. M. Poskanzer, A. Sandoval, R. Stock, and G. D. Westfall, Phys. Rev. C **16**, 629 (1977).

²V. Perez-Mendez, A. L. Sagile, E. T. B. Whipple, F. Zarbakhsh, G. Igo, M. M. Gazzaly, J. B. Carroll, J. V. Geaga, J. B. McClelland, M. A. Nasser, H. Spinka, and R. Talaga, Lawrence Berkeley Laboratory Report No. LBL-7278 (unpublished).

³S. Nagamiya, I. Tanihata, S. Schmetzer, L. Anderson, W. Brückner, O. Chamberlain, G. Shapiro, and H. Steiner, Lawrence Berkeley Laboratory Report No. LBL-6770 (unpublished).

⁴K. Nakai, J. Chiba, I. Tanihata, S. Nagamiya, H. Bowman, J. Ioannou, and J. O. Rasmussen, in Proceedings of the International Conference on Nuclear Structure, Tokyo, 1977 (unpublished), Vol. 3; and private communication.

⁵For a comparison of the different models see M. Gyulassy, Lawrence Berkeley Laboratory Report, No. LBL-6594 (unpublished); and in Proceedings of International Symposium on Nuclear Collisions and their Microscopic Description, Bled, Yugoslavia, 1977 (unpublished).

⁶G. D. Westfall, J. Gosset, P. J. Johansen, A. M. Poskanzer, W. G. Meyer, H. H. Gutbrod, A. Sandoval, and R. Stock, Phys. Rev. Lett. **37**, 1202 (1976), and Ref. 1.

⁷W. D. Myers, Nucl. Phys. **A296**, 177 (1978). Myers coined the word firestreak to refer to this model when thermal distributions are used.

⁸R. K. Smith and M. Danos, in Proceedings of Meeting on Heavy Ion Collisions, Fall Creek Falls, 1977 (unpublished); and (unpublished).

⁹A. A. Amsden, J. N. Ginocchio, F. H. Harlow, J. R. Nix, M. Danos, E. C. Halbert, and R. K. Smith, Phys.

Rev. Lett. **38**, 1055 (1977).

¹⁰J. P. Bondorf, H. T. Feldmeier, S. Garpmann, and E. C. Halbert, Phys. Lett. **65B**, 217 (1976); Z. Phys. **279**, 385 (1976).

¹¹A. A. Amsden, F. H. Harlow, and J. R. Nix, Phys. Rev. C **15**, 2059 (1977).

¹²J. Hüfner and J. Knoll, Nucl. Phys. **A290**, 460 (1977).

¹³S. E. Koonin, Phys. Rev. Lett. **39**, 680 (1977).

¹⁴H. H. Gutbrod, A. Sandoval, P. J. Johansen, A. M. Poskanzer, J. Gosset, W. G. Meyer, G. D. Westfall, and R. Stock, Phys. Rev. Lett. **37**, 667 (1976) and Ref. 1.

¹⁵A. J. Mekjian, Phys. Rev. Lett. **38**, 640 (1977); Phys. Rev. C **17**, 1051 (1978).

¹⁶J. Bond, P. J. Johansen, S. E. Koonin, and S. Garpmann, Phys. Lett. **71B**, 43 (1977).

¹⁷J. I. Kapusta, Phys. Rev. C **16**, 1493 (1977).

¹⁸See Ref. 1 and references therein.

¹⁹In principle there could be effects which depend on the length of the streaks, for instance, if one does not assume completely inelastic collisions between streaks.

²⁰E. Segrè, *Nuclei and Particles* (Benjamin, New York, 1964), p. 635.

²¹S. Fiarman and S. S. Hanna, Nucl. Phys. **A251**, 1 (1975).

²²S. Fiarman and W. E. Meyerhof, Nucl. Phys. **A206**, 1 (1973).

²³F. Ajzenberg-Selove and T. Lauritsen, Nucl. Phys. **A227**, 1 (1974).

²⁴The computer code written to perform the calculations described in this section is available.

²⁵This is in contrast to the coalescence model which requires a separate parameter for each nuclear fragment. This parameter also varies somewhat with beam energy. See Ref. 1 and references therein.

²⁶See Ref. 1. We thank the authors for allowing us the use of some of their unpublished data.

²⁷In this regard see M. Gyulassy and S. K. Kauffmann, Phys. Rev. Lett. **40**, 298 (1978).